UNIVERSITY OF CALIFORNIA SAN DIEGO

Effects of *Ankrd16* loss in motor neurons of aminoacyl tRNA synthetase editing-deficient mice

A Thesis submitted in partial satisfaction of the requirements for the degree

Master of Science

in

Biology

by

Connor Foreman

Committee in charge:

Professor Susan Ackerman, Chair
Professor Brenda Bloodgood
Professor Yishi Jin

2021

The Thesis of Connor Foreman is approved, and it is acceptable in quality and form for publication on microfilm and electronically.

University of California San Diego

2021

TABLE OF CONTENTS

LIST OF FIGURES

ACKNOWLEDGEMENTS

I would like to express my deepest and most sincere gratitude to Professor Susan Ackerman and Alana Gibson for their tremendous support throughout my journey in research. Without their guidance and patience as a mentor and willingness to answer my limitless questions, this thesis would not have been possible.

I would also like to thank Professor Brenda Bloodgood and Professor Yishi Jin for being a part of my thesis committee.

In addition, I would like to thank every member of the Ackerman lab for all of their help and assistance with any of my experiments.

Last but not least, I would like to thank my parents, Mr. and Mrs. Foreman, for their unconditional love, support, and sacrifices for educating and preparing me for the future. Without them, I wouldn't have been able to make it this far.

ABSTRACT OF THE THESIS

Effects of *Ankrd16* loss in motor neurons of aminoacyl tRNA synthetase editing-deficient mice

by

Connor Foreman

Master of Science in Biology

University of California San Diego, 2021

Professor Susan Ackerman, Chair

Errors in tRNA aminoacylation can lead to misfolded proteins, which can form protein aggregates. Protein aggregation has been linked to many neurological diseases, thus understanding the mechanisms that can lead to the formation of protein aggregates is critical for researching degenerative illnesses. Aminoacyl tRNA synthetases (AARSs) have been found to have hydrolytic editing functions that can correct tRNA mischarging errors and prevent

mistranslation. A mutation, referred to as sticky, has been discovered to cause a dysfunction in the hydrolytic editing function of alanyl-tRNA synthetase (AlaRS), resulting in mischarged Ser-tRNA^{Ala} and causes serine to be incorrectly incorporated into newly-formed peptides. However, ANKRD16, a newly discovered protein, has been found to aid AlaRS in editing of mischarged tRNAs by removing serine from the aminoacyl active site of AlaRS. By conditionally deleting *Ankrd16* in CaMKIIa-expressing neurons in the forebrain of *Aars*$^{sti/sti}$ mice, the Ackerman lab was able to induce neuronal death in targeted neurons (Vo et al., 2018). In this study, we attempted to induce motor neuron death by conditionally deleting *Ankrd16* in motor neurons of *Aars*$^{sti/sti}$ mice. Although motor neuron death was not observed, other phenotypes, such as decreased weight, kyphosis, and decreased axon diameters were found to be caused by the conditional deletion of *Ankrd16*. These results suggest that motor neurons may be more resistant to *Ankrd16* loss than other neurons, such as Purkinje cells.

Introduction

Errors in tRNA aminoacylation can lead to misfolded proteins.

The process of tRNA aminoacylation is one of the first steps of protein synthesis and is carried out by enzymes referred to as aminoacyl tRNA synthetases (AARSs) (Pang et al., 2014). Each AARS is specifically designed to attach a distinct amino acid to its corresponding cognate tRNA in a two-step reaction (Newberry et al., 2002; Pang et al., 2014). First these enzymes catalyze the reaction of their cognate amino acid with ATP to form an aminoacyl adenylate (AA-AMP) intermediate. During this step, ATP loses two phosphates, and the amino acid becomes covalently attached to AMP. AMP is released during the second step of tRNA aminoacylation, when a tRNA binds to the AARS. The AARS then utilizes this energy to attach the amino acid to the tRNA.

Mammalian cells have developed numerous checks and balances to preserve translational fidelity and maintain a low rate of amino acid misincorporation during protein synthesis (one in every 10,000 codons) (Jakubowski & Goldman, 1992). While aminoacyl tRNA synthetases can maintain high levels of fidelity, every so often a mistake can occur during tRNA aminoacylation which can lead to misincorporation of the wrong amino acid into the nascent polypeptide chain during translation and cause misfolded proteins (Lee et al., 2006).

Aminoacyl tRNA synthetases have hydrolytic editing functions that can correct errors.

While AARSs are not only responsible for recognizing tRNAs with the correct anticodon, they must also select for the cognate amino acid (Jakubowski & Goldman, 1992). In general, tRNAs are distinguished by specific identity elements such as nucleotide modifications,

however, amino acids are small molecules, and can sometimes differ by only a single methyl group (Giegé et al., 1998; Pang et al., 2014). This makes it extremely difficult for AARSs to distinguish between amino acids and can cause a noncognate amino acid to be mistakenly activated in a process known as misactivation. If not corrected, misactivated amino acids can be then charged to a non-cognate tRNA. This is typically referred to as mischarging.

The aminoacyl active site of an AARS is considered the first checkpoint of editing as it selects for size and chemical properties of amino acids. It excludes amino acids that are larger than the amino acid of interest and only allows smaller or similar size amino acids to bind (Moras, 2010). In addition to selecting for size, the active site only allows amino acids that have the correct chemical properties, such as charge. Despite the fact that selectivity of amino acids exists in AARSs, certain amino acids are more prone to being mischarged than others owing to their similarity in form and physical characteristics (Guo et al., 2009; Pang et al., 2014). When selectivity at the catalytic site fails and a noncognate amino acid becomes misadenylated, the AARS utilizes its hydrolytic editing capabilities.

It is estimated that about half of the AARS enzymatic family have hydrolytic editing functions, which keep rates of misincorporation in the production of proteins within acceptable limits (Dulic et al., 2010; Pang et al., 2014). The AARSs that have trouble differentiating certain amino acids due to similarities in size and charge are more likely to have hydrolytic editing capabilities. The proposed method for AARSs to achieve and maintain their fidelity is through two different editing pathways: pre-transfer and post-transfer of the amino acid onto the tRNA (Hopfield, 1974). Pre-transfer editing occurs at the aminoacyl active site and or at a separate editing site and is characterized by the recognition and hydrolysis of noncognate AA-AMP by

AARSs prior to the transfer of the amino acid onto a tRNA, thus preventing the formation of mischarged tRNAs (Dulic et al., 2010; Martinis & Boniecki, 2008).

Although aminoacyl tRNA synthetases have evolved the ability to remove amino acids from the active site, they can still make errors and mischarge tRNAs (Newberry et al., 2002). Thus, to overcome this issue, aminoacyl tRNA synthetases have acquired the ability of post-transfer editing which occurs after the mischarged amino acid is attached to the wrong tRNA. Post-transfer editing takes place in the editing domain of AARSs and works by hydrolyzing the mischarged amino acid off of the noncognate tRNA (Dulic et al., 2010; Martinis & Boniecki, 2008). By removing mischarged amino acids, AARSs are able to prevent mistranslation.

Misfolded proteins can lead to neurodegenerative diseases.

The underlying causes of neurodegenerative diseases are largely undetermined, but protein aggregates are often associated with these diseases and are hypothesized to contribute to neuronal death (Davis & Stroud, 2013). This makes the study of protein aggregates highly integral in combating neurodegenerative diseases. Severity of neurodegenerative disease is correlated with the accumulation of protein aggregates. In numerous neurodegenerative diseases, aggregates of specific proteins can be found in neurons in particular areas of the nervous system and cause a wide variety of neurological defects. For example, some patients with amyotrophic lateral sclerosis (ALS) have dominant mutations in superoxide dismutase-1 (SOD1) which causes abnormal accumulation of this aberrant protein specifically in motor neurons (Benkler et al., 2018). While the structure and composition of protein aggregates is not fully understood, it is broadly believed that they are the accumulation of misfolded proteins (Davis & Stroud, 2013). In general it is thought that mature neurons are more susceptible to cell death by protein

aggregation because they are unable to divide like many other cell types in the body (Frade & Ovejero-Benito, 2015). Cell division is proposed to divide protein aggregates amongst daughter cells and thus can become an effective method for diluting misfolded proteins (Schramm et al., 2019).

Sticky mice have a mutation in the editing domain of alanyl-tRNA synthetase.

In one of the first studies examining the consequences of loss of aminoacyl tRNA synthetase editing in eukaryotes, the Ackerman lab demonstrated that a mutation in the *Aars* gene, which encodes for an alanyl-tRNA synthetase (AlaRS), disrupts its hydrolytic editing function. In particular, this spontaneous mouse mutation, referred to as the *sticky (sti)* mutation, caused an alanine to glutamic acid substitution at amino acid 734 in the editing domain of AlaRS and disrupts its pre-transfer editing capabilities (Lee et al., 2006; Vo et al., 2018). Normally, AlaRS is responsible for facilitating the charging of alanine onto cognate $tRNA^{Ala}$ and forming Ala-$tRNA^{Ala}$ (Sokabe et al., 2009). However, this disruption in pre-transfer editing causes the aminoacyl tRNA synthetase to occasionally misactivate the non-cognate amino acid serine and subsequently produce mischarged Ser-$tRNA^{Ala}$ (Lee et al., 2006). The *sticky* mutation prevents effective editing of misactivated serine and serine can be incorporated at alanine codons into nascent proteins (Vo et al., 2018). The formation of protein aggregates has been observed $Aars^{sti/sti}$ mice, likely caused by protein folding defects due to the misincorporation of serine (Lee et al., 2006). Despite the presence of AlaRS in every neuron and all other somatic cells, ubiquinated protein aggregates were only found in cerebellar Purkinje cells of $Aars^{sti/sti}$ mutant mice, which progressively degenerate. Consequently, due to the loss of Purkinje cells, these mice

also develop cerebellar ataxia, displaying impairment of balance and coordination (Lee et al., 2006).

Ankrd16 can rescue *sticky* mutant mice.

While genetically mapping the *sticky* mutation, the Ackerman lab discovered that when *Aars*$^{sti/+}$ mice on the inbred C57BL/6J (B6J) background were crossed with CAST/Ei (CAST) or CASA/RkJ (CASA) mice and then backcrossed to B6J; *Aars*$^{sti/+}$ mice, 50% of the offspring did not exhibit ataxia or Purkinje cell degeneration (Vo et al., 2018). This suppression of the *sticky* mutation was not seen with crosses in any other inbred strains of mice (BALB/cJ, C3H/HeJ, DBA/2J, MOLF/Ei), which suggested that alleles derived from CAST or CASA are capable of suppressing neuron loss. The Ackerman lab localized the modifier of *sticky* to a 0.63-Mb region on chromosome 2 and further genetic mapping identified the modifier to be a SNP occurring in intron 5 of the gene *Ankrd16*. This SNP is a hypomorphic mutation and causes an alternative splice site in *Ankrd16* transcripts, which produces a 138-bp cryptic exon (exon 5') containing a premature stop codon. These mutant *Ankrd16* transcripts end at the cryptic exon 5' and are predicted to undergo nonsense-mediate decay, resulting in a 3.9 fold decrease in B6J ANKRD16 protein levels when compared to CAST ANKRD16 protein levels (Vo et al., 2018). It was then discovered that the SNP in *Ankrd16* was only observed in non-rescuing strains but was absent in CAST or CASA. Transgenic expression of the CAST *Ankrd16* allele in *Aars*$^{sti/sti}$ mice on a B6J background was successful in suppressing Purkinje cell degeneration, confirming that *Ankrd16* is the gene that suppresses the *sticky* mutation.

The newly discovered protein, ANKRD16, encoded by the *Ankrd16* gene, acts as a co-regulator for the editing domain of AlaRS. ANKRD16 is a 39 kDa protein consisting of nine

repeating ankyrin domains, domains that function to mediate protein-protein interactions (Vo et al., 2018). The Ackerman lab demonstrated that during dipeptide formation experiments, in the absence of ANKRD16, mutant AlaRS was mischarging $tRNA^{Ala}$ with serine, while also charging $tRNA^{Ala}$ with alanine. However, addition of ANKRD16 to the dipeptide formation experiment resulted in nearly no mischarged Ser-$tRNA^{Ala}$, and instead correctly charged Ala-$tRNA^{Ala}$, suggesting that ANKRD16 co-regulates the editing functions of AlaRS.

During aminoacylation assays, ANKRD16 was found to interact with serine but not with alanine in the presence of $tRNA^{Ala}$ and mutant AlaRS. It is therefore believed that ANKRD16 functions as an alternative to $tRNA^{Ala}$ and accepts misactivated serine. In addition, co-IP experiments revealed that ANKRD16 interacts with the aminoacylation domain and not the editing domain of AlaRS. Altogether, this data suggests that ANKRD16 binds and removes misactivated serine at the active site of AlaRS, thus halting the production of Ser-$tRNA^{Ala}$ and preventing the incorporation of mischarged amino acids (Vo et al., 2018).

Neuronal death can be induced by conditionally deleting *Ankrd16*

Although ANKRD16 is ubiquitously expressed, ANKRD16 levels are relatively lower in Purkinje cells of B6J.*Ankrd16*$^{CAST/CAST}$ when compared to other neuronal cell types. B6J.*Ankrd16*$^{CAST/CAST}$ are congenic mice that have the *Ankrd16* allele from CAST but are B6J at every other allele and were used since B6J contains a SNP in the *Ankrd16* gene. This suggests that the reason Purkinje cell-specific death occurs in *Aars*$^{sti/sti}$ mutants is because Purkinje cells are particularly sensitive to the *sticky* mutation due to their low levels of endogenous ANKRD16. To determine if the specificity of neuron death in *Aars*$^{sti/sti}$ mice is affected by the levels of ANKRD16, the Ackerman lab conditionally deleted *Ankrd16* in postnatal Purkinje cells in

Aars$^{sti/sti}$ mice using a Cre-loxP system (Vo et al., 2018). The conditional allele was created by flanking exon 2 of the *Ankrd16* gene with loxP sites. These loxP sites are excised by Cre, which was expressed under the control of the *Pcp2* (Purkinje cell protein-2) promoter, which expresses highly in cerebellar Purkinje cells. Conditional deletion of *Ankrd16* by Pcp2-Cre in *Aars*$^{sti/sti}$ mice was found to result in cell death of Purkinje cells at about 3 weeks of age. In comparison, *Aars*$^{sti/sti}$ mice display Purkinje cell degeneration beginning at 4 weeks of age, indicating that conditional deletion of *Ankrd16* in Purkinje cells caused a more severe phenotype. At 4 weeks of age, the majority of Purkinje cells in these mice were almost completely absent, and by 7 months of age, all Purkinje cells were deteriorated. These results suggests that levels of ANKRD16 influence the cell survival of Purkinje cells in *Aars*$^{sti/sti}$ mice and conditional deletion of *Ankrd16* further worsens Purkinje cell degeneration.

To test if altered ANKRD16 levels combined with the *sticky* mutation can induce neuronal death in cell types that have thus far been resistant to cell death, the Ackerman lab conditionally deleted *Ankrd16* in excitatory neurons in the forebrain using Cre expressed under the control of a CaMKIIa promoter. Conditional deletion of *Ankrd16* by CaMKIIa-Cre in *Aars*$^{sti/sti}$ mice was found to result in protein aggregation and cell death of cortical and hippocampal forebrain neurons. These results demonstrate that alterations in *Ankrd16* levels can affect neurons other than Purkinje cells, suggesting that we can use the conditional *Ankrd16* allele and the *Aars*$^{sti/sti}$ mutation to drive cell-type specific aggregation and neurodegeneration (Vo et al., 2018).

Are motor neurons susceptible to mistranslation?

Since we knew that we could drive cell death by lowering ANKRD16 levels in many forebrain neurons, we wanted to see if we could drive protein aggregation and neuronal death in other neuronal populations as well. We attempted to use the *Ankrd16 / Aars*$^{sti/sti}$ strategy to generate a mouse model of motor neuron death with aggregate formation of endogenous proteins. We targeted motor neurons because loss of these neurons leads to a specific behavioral readout of impaired motor movement. To drive mistranslation in motor neurons in the spinal cord, a Cre under the control of a choline acetyltransferase (ChAT) promoter was used to delete *Ankrd16* in these neurons in *Aars*$^{sti/sti}$ mice. The goal of my project was to determine the phenotypic consequences of *Ankrd16* deletion in *Aars*$^{sti/sti}$ mice.

Materials and Methods

Mice.

Homologous recombination of the *Ankrd16* locus was performed to generate mice with the targeted *Ankrd16* allele as previously described (Vo et al., 2018). Mice were backcrossed to C57BL6/J for 10 generations. *Ankrd16*$^{neo/+}$ mice were crossed to B6.FVB-Tg(EIIa-cre) C5379Lmgd/J (The Jackson Laboratory, stock #003724) to generate the *Ankrd16*$^{+/-}$ allele. To generate a conditional *Ankrd16*$^{fl/-}$ allele, the neo cassette was removed by crossing *Ankrd16*$^{neo/+}$ mice to B6.129S4-Gt(ROSA)26Sor$^{tm1(FLP1)Dym}$/RainJ (The Jackson Laboratory, stock #009086). Knock-in Cre mice with the Cre recombinase gene inserted downstream of the stop codon for the ChAT gene (B6; 129S6-ChAT$^{(tm2(cre)Lowl)/J}$, The Jackson Laboratory, stock #031661) were acquired from The Jackson laboratory. To allow for Cre recombinase translation, an internal ribosome entry site was added before the Cre recombinase gene. The *sticky* mutation emerged spontaneously in an unknown stock mouse, which was then transferred to the C57BL/6J (B6J) background (Lee et al., 2006). B6J.*Ankrd16*$^{CAST/CAST}$ and *Ankrd16*$^{-/-}$ were created as previously described (Vo et al., 2018).

Genotyping was performed on tail tissue samples from mice that were approximately 3 weeks old. 120 µl of 50 mm NaOH was added to tail samples and tissue was placed at 95°C for 15 minutes. 30 µl of 1M tris/5 mM EDTA was then added to tail samples. To genotype for the *sticky* mutant mutation, the primers were: mutant forward 5’ CTACGGAATTCTAGCCATGA 3’ and common reverse 5’ TGTGTACATGGTACATATGT 3’. To genotype for the *sticky* wild type allele, the primers were: wild-type forward 5’ CTACGGAATTCTAGCCATGC 3’ and common reverse 5’ TGTGTACATGGTACATATGT 3’. For both *sticky* mutant and wild type,

the amplification procedure was as follows: (1) 94°C for 3 minutes (2) 94°C for 30 seconds (3) 55°C for 30 seconds (4) 72°C for 30 seconds (5) repeat steps 2-4 40x, then 72°C for 10 minutes (6) and 10°C for 10 minutes. Cr1a forward 5' ATTGCTGTCACTTGGTCGTGGC 3' and Cr2a reverse 5' GGAAAATGCTTCTGTCCGTTTGC 3' were used to genotype for *ChAT-Cre*. For amplification of *ChAT-Cre*, the procedure was as follows: (1) 94°C for 2 minutes (2) 94°C for 20 seconds (3) 60°C for 30 seconds (4) 72°C for 30 seconds (5) repeat steps 2-4 33x, then 72°C for 10 minutes (6) and 4°C for 10 minutes. To genotype for *Ankrd16*, three primers were used: AnkloxPDelR 5' GACCCTGACTCCATGAACTGC 3', KOloxPR-2 5' TGTTTTCAGTGGTGGGAGAG 3', and AnkloxPF 5' CGCCATGCACCGAATATTGA 3'. For amplification of *Ankrd16*, the procedure was as follows: (1) 94°C for 4 minutes (2) 94°C for 30 seconds (3) 60°C for 30 seconds (4) 72°C for 30 seconds (5) repeat steps 2-4 39x, then 72°C for 10 minutes (6) 10°C for 10 minutes. For *sticky* and *ChAT-Cre*, PCR products were visualized on 1.5% agarose gel. For *Ankrd16*, PCR products were visualized on 4% agarose gel. The PCR product size for wild type and mutant *sticky* bands are approximately ~350 bp and ~200 bp for Cre. For *Ankrd16*, the PCR product size for wild type is ~100 bp, floxed *Ankrd16* is ~150 bp, and deletion of *Ankrd16* is ~200 bp.

BaseScope *in situ* hybridization.

BaseScope 3 ZZ probes from ACD Bio were specifically designed to detect the conditionally deleted exon 2 (nucleotides 1151-1281) of the *Ankrd16* transcript (NM_177268.4). Anesthetized mice were perfused and spinal cords were post-fixed overnight with neutral buffered formalin (NBF) and embedded in paraffin. Tissues were then sectioned via microtome at 7 µm thin. Spinal cord sections were collected at C7. Sections were then deparaffinated via

autostainer following standard procedures. Sections were treated with hydrogen peroxidase for 10 minutes at room temperature. Target retrieval was performed by boiling spinal cord sections in RNAscope target retrieval solution at 99°C for 30 minutes. Slides were then transferred to alcohol for 3 minutes, followed by drying in a 60°C incubator for 5 minutes. RNAscope Protease IV was placed on spinal cord sections for 30 minutes. Sections were then hybridized with the designed 3 ZZ probes for 2 hours in a 40°C incubator, followed by a 2-minute wash in 1X wash buffer at room temperature. Hybridized slides were amplified with BaseScope v2 AMP 1-8 according to manufacturer's protocol, with the exception of BaseScope v2 AMP 7 which was treated for 45 minutes on spinal cord sections at room temperature. BaseScope Fast RED was used for signal detection and was placed on slides for 10 minutes at room temperature. Slides were immediately blocked in 5% goat serum in PBST and incubated in rabbit anti-ChAT (1:1000, Abcam, cat# ab177850) overnight at 4°C. Sections were then rinsed 3 times for 15 minutes each in PBST. Secondary antibodies, goat anti-rabbit 488 IgG (H+L) (1:500, Invitrogen, cat# A11034), were placed on sections for 2 hours at 4°C. Slides were then rinsed 2 times for 10 minutes each in PBS. Slides were counterstained with RNAscope DAPI , followed by coverslipping using standard procedures. Sections were then imaged using a Zeiss fluorescent microscope (Axio Observer Z1).

Motor Neuron Quantification.

Mice were perfused with 4% PFA, followed by collection of the spinal cord. The spinal cord in the vertebral column was then post-fixed overnight in 4% PFA. A laminectomy was performed, and the cervical region was embedded in paraffin and serially sectioned at 7 µm. To locate sections from the seventh cervical vertebra (C7), every sixth section was stained with

cresyl violet according to standard procedures. Cresyl violet-stained cervical sections were then section matched using the Allen Spinal Cord Atlas. Once the C7 region was determined, slides from that region were collected for immunohistochemistry.

Immunofluorescence of C7 sections was performed using a tyramide signal amplification (TSA) protocol. Deparaffination was performed on sections following standard procedures. Sections were then placed in PBS for 20 minutes. Antigen retrieval was performed by microwaving sections in a citric acid buffer solution on 20% power (1200 watts at 100% power), three times for three minutes each with 1 minute rest in between cycles. Sections were then cooled down for 30 minutes. Sections were blocked with 5% goat serum in PBST for 1 hour. Immunofluorescence of ChAT was performed by incubating sections with rabbit anti-ChAT (1:1000, Abcam, cat# ab177850) overnight at 4°C. Sections were then rinsed 3 times for 5 minutes each in PBST. Secondary antibodies, goat anti-mouse IgG (H+L)-HRP conjugate (Bio-Rad, cat# 170-6516), were placed on sections for 1 hour at room temperature. Slides were then rinsed 3 times for 5 minutes each in PBST. TSA plus Cy3 (Perkin Elmer) diluted (1:50) in amplification buffer was then placed on slides for 5 minutes. They were then washed 3 times for 5 minutes each in PBST. Sections were stained with DAPI (1 μg/ml) for 10 minutes, washed in PBS for 10 minutes, and incubated with Sudan black for 10 minutes to reduce autofluorescence and then washed for 10 minutes in PBS. Slides were then coverslipped following standard procedures. Once C7 sections were stained and coverslipped, they were imaged by a Zeiss fluorescent microscope (Axio Observer Z1). C7 section images were randomized, and ChAT-expressing motor neurons were blindly quantified. To obtain an average number of motor neurons, 3 C7 sections greater than 35 microns apart from each other were quantified for each mouse. After quantification, data was put into GraphPad Prism 7.0 for statistical analysis.

Femoral/L5 Axon Quantification.

Mice were first perfused with EM fixative (2% PFA + 2.5% glutaraldehyde in 0.15M sodium cacodylate buffer). The femoral nerve and L5 ventral root were then dissected and post-fixed in EM fixative overnight and then transferred to PBS. Tissues were then sent to The Jackson Laboratory for sectioning at 500 nm and staining with Toluidine Blue. Tissues were imaged at 40x using an Olympus BX50 microscope. Quantification of number of axons in the femoral nerve and L5 ventral root was performed by using the cell counter plugin on FIJI (Fiji Is Just ImageJ). Quantification of axon diameter and g-ratio was performed by measuring the inner diameter (diameter of axon without myelination) and outer diameter (diameter of axon including myelination) of axons in the femoral nerve. The shortest inner and outer axon diameter was measured for axons that were not round. To calculate g-ratio, each axon's inner diameter was divided by the outside diameter. Data was then put into GraphPad Prism 7.0 for statistical analysis.

Muscle Weights and Neuromuscular Junction assay.

The plantaris, gastrocnemius and triceps muscles were collected from anesthetized mice, and the gastrocnemius and triceps were weighed. Muscles were drop-fixed in 2% PFA for two hours on ice and then placed in PBS. Tissues were embedded in 4% low-melt agarose and sectioned at 75 µm. Sections were blocked with 5% goat serum + 0.5% PBS-Triton for 1 hour on a shaker. Sections were placed in primary antibody solution, mouse anti-2H3 neurofilament (1:500, DSHB ascites) + mouse anti-SV2 (1:500, DHSB ascites), overnight in a cold room on a shaker. The next day, sections were washed every hour with 0.5% PBST for 7 hours. After, they

were placed in a secondary antibody solution, goat anti-mouse 488 IgG1 (1:500, Thermo Fisher Scientific, cat# A-21121) + anti-alpha-bungarotoxin-594 (1:500, Molecular Probes, cat# B-13423), overnight in a cold room on a shaker. Sections were then washed every hour with 0.5% PBST for 7 hours. After 7 hours of washing, sections were mounted, and coverslipped following standard procedures. Stained sections were then imaged using a Zeiss fluorescent microscope (Axio Observer Z1) and Apotome. Using the Apotome, images of a single NMJ were taken at multiple z-planes and were merged into a single image. NMJs of each genotype were qualitatively assessed for NMJ defects.

Results

Ankrd16 is expressed in the motor neurons of B6J.*Ankrd16*$^{CAST/CAST}$ mice.

To determine if *Ankrd16* is expressed in motor neurons, I performed BaseScope *in situ* hybridization on a B6J.*Ankrd16*$^{CAST/CAST}$ mouse containing the *Ankrd16* allele from the CAST mouse strain. Expression levels of *Ankrd16* transcripts in the cerebellum of CAST mice were found to be 5.3-fold higher than B6J mice (Vo et al., 2018), however, levels are unknown in motor neurons. A 3 ZZ BaseScope probe was designed to target exon 2 (nucleotides 1151-1281) of the *Ankrd16* transcript (NM_177268.4). 3 ZZ refers to the number of double Z probes that adhere to the RNA target, with each Z probe containing a region complementary to *Ankrd16* exon 2, a spacer region, and pre-amplifier region that allows for signal amplification (Wang et al., 2012). After qualitative evaluation, I observed *Ankrd16* transcripts in the motor neurons of B6J.*Ankrd16*$^{CAST/CAST}$ mice (Fig. 1a-d). I also did not observe *Ankrd16* transcripts in the motor neurons of *Ankrd16*$^{-/-}$ mice (Fig. 1e-h), confirming the specificity of the probes. These results indicate that wild-type *Ankrd16* is expressed in motor neurons.

Ankrd16 was conditionally deleted in *ChAT-Cre; Ankrd16*$^{fl/-}$*; Aars*$^{sti/sti}$ mice.

In order to generate the *ChAT-Cre; Ankrd16*$^{fl/-}$*; Aars*$^{sti/sti}$ mutants, a specific order of crosses was carried out by Alana Gibson (Fig. 2). First, *Ankrd16*$^{-/-}$ were mated with *ChAT-Cre* mice and intercrossed to generate *ChAT-Cre; Ankrd16*$^{-/-}$. *ChAT-Cre; Ankrd16*$^{-/-}$ were then mated with *Aars*$^{sti/+}$ and intercrossed to generate *ChAT-Cre; Ankrd16*$^{-/-}$*; Aars*$^{sti/+}$. *Aars*$^{sti/+}$ mice were used due to infertility issues with *Aars*$^{sti/sti}$. *Ankrd16*$^{fl/fl}$, which are mice that have *Ankrd16* floxed with loxP sites, were then mated with *Aars*$^{sti/+}$ and intercrossed to generate *Ankrd16*$^{fl/fl}$*; Aars*$^{sti/+}$.

Lastly, *ChAT-Cre; Ankrd16$^{-/-}$; Aars$^{sti/+}$* is crossed with *Ankrd16$^{fl/fl}$; Aars$^{sti/+}$* to generate *ChAT-Cre; Ankrd16$^{fl/-}$; Aars$^{sti/sti}$* mutants (Fig. 2).

To test if lower levels of ANKRD16 combined with the *sticky* mutation could induce cell death in motor neurons, the Ackerman lab conditionally deleted exon 2 of *Ankrd16* in motor neurons of *Aars$^{sti/sti}$* mice using a floxed *Ankrd16* allele and B6; 129S6-*ChAT$^{(tm2(cre)Lowl)/J)}$* Cre mice, in which the Cre recombinase gene is inserted downstream of the stop codon for the Choline Acetyltransferase (ChAT) gene. *ChAT-Cre* mice were obtained from The Jackson Laboratory. An internal ribosome entry site (IRES) was also added by The Jackson Laboratory before the Cre recombinase gene to allow for Cre recombinase translation. This allows for Cre to be expressed in cells, such as spinal motor neurons, that express endogenous ChAT.

To confirm that *Ankrd16* was conditionally deleted in motor neurons, I performed BaseScope *in situ* hybridization on *ChAT-Cre; Ankrd16$^{fl/-}$; Aars$^{sti/sti}$* mice. *In situ* hybridization revealed that *Ankrd16* was not present in the motor neurons of *ChAT-Cre; Ankrd16$^{fl/-}$; Aars$^{sti/sti}$* mice (Fig. 1i-l), however *Ankrd16* was expressed in other cells in the spinal cord (data not shown). This indicates that *Ankrd16* was conditionally deleted in motor neurons of *ChAT-Cre; Ankrd16$^{fl/-}$; Aars$^{sti/sti}$* mice.

Loss of *Ankrd16* in motor neurons of *Aars$^{sti/sti}$* mice results in kyphosis and decreased body and muscle weight.

ChAT-Cre; Ankrd16$^{fl/-}$; Aars$^{sti/sti}$ mice were aged by Alana Gibson to look for age-dependent phenotypes and were found to have a life expectancy of 9-10 months old. Thus, all studies were done in mice at 8 months of age. Like *Aars$^{sti/sti}$* mice, *ChAT-Cre; Ankrd16$^{fl/-}$; Aars$^{sti/sti}$* mice displayed tremors as defined by their inability to control the direction of their

movements (data not shown). No signs of motor abnormalities were observed in *ChAT-Cre; Ankrd16$^{fl/-}$* or wild-type C57BL/6J (B6J) mice. When qualitatively compared to B6J, *ChAT-Cre; Ankrd16$^{fl/-}$*, and *Aars$^{sti/sti}$* mice, *ChAT-Cre; Ankrd16$^{fl/-}$; Aars$^{sti/sti}$* mice appeared smaller and were kyphotic (data not shown). *Aars$^{sti/sti}$* mice have been previously shown to be smaller than wild-type B6J mice at 6 weeks of age (Lee et al., 2006) and indeed these mice weighed less than wild-type at 8 months of age (Fig. 3a, 3b). 8-month-old *ChAT-Cre; Ankrd16$^{fl/-}$; Aars$^{sti/sti}$* mice weighed even less than *Aars$^{sti/sti}$* mice (Fig. 3a, 3b) suggesting that kyphosis and decreased weights are caused by conditional deletion of *Ankrd16* in motor neurons in *Aars$^{sti/sti}$* mice.

Since the axons of motor neurons ultimately innervate muscles, weights of muscles were analyzed to assess potential muscle defects in *ChAT-Cre; Ankrd16$^{fl/-}$; Aars$^{sti/sti}$* mutant mice at 8 months of age. The triceps and gastrocnemius muscles were dissected and weighed by Alana Gibson. Once I received the muscle weights, I divided muscle weights by the total body weight of corresponding mice to get the muscle-to-body weight ratio. By using the muscle-to-body weight ratio of each genotype, we can determine if muscle weights change disproportionally to total body size. Quantification of the muscle-to-body weight ratios revealed a significant decrease in the triceps and gastrocnemius muscles relative to total body weight of *ChAT-Cre; Ankrd16$^{fl/-}$; Aars$^{sti/sti}$* mice, when compared to B6J, *ChAT-Cre; Ankrd16$^{fl/-}$*, and *Aars$^{sti/sti}$* (Fig 4a, 4b) indicating that these muscles may fail to grow normally or may atrophy.

Neuromuscular Junction Morphology appears normal in *ChAT-Cre; Ankrd16$^{fl/-}$; Aars$^{sti/sti}$* mice.

To further investigate pathology in the muscle, we next decided to investigate any potential issues at the neuromuscular junction (NMJ). The NMJ is the site at which motor axon

terminals synapse onto muscle fibers and the area at which transmission of action potentials occurs. We reasoned that motor axon dysfunction in *ChAT-Cre; Ankrd16$^{fl/-}$; Aars$^{sti/sti}$* mutant mice may be occurring at the presynaptic nerve terminal of the NMJ causing muscles to atrophy. The plantaris, gastrocnemius, and triceps were collected by Alana Gibson, and I qualitatively analyzed NMJ morphology by staining the muscles of B6J, *ChAT-Cre; Ankrd16$^{fl/-}$*, *Aars$^{sti/sti}$*, and *ChAT-Cre; Ankrd16$^{fl/-}$; Aars$^{sti/sti}$* mutant mice with 2H3 (neurofilament) and SV2 (synaptic vesicles) antibodies to label the presynaptic axon and nerve terminal, and α-bungarotoxin to label the postsynaptic muscle end plate. An absence or deterioration of nerve terminals in *ChAT-Cre; Ankrd16$^{fl/-}$; Aars$^{sti/sti}$* mutant mice would suggest that decreased muscle weights could be due to dysfunction or death of motor neurons. After evaluation, there was no qualitative difference in NMJ morphology detected between *ChAT-Cre; Ankrd16$^{fl/-}$; Aars$^{sti/sti}$* mutant and control mice (Fig. 5a-f). This suggests that the decrease in muscle weight in these mice is not due to denervation of NMJs.

Conditionally deleted *Ankrd16* in *Aars$^{sti/sti}$* motor neurons does not induce their loss.

To determine if lower motor neuron death is induced by conditional deletion of *Ankrd16* in motor neurons of *Aars$^{sti/sti}$* mice, Alana Gibson collected the cervical region of the spinal cord, and I sectioned the cervical region to the seventh cervical vertebrate. I then performed immunofluorescence to label motor neurons using an anti-ChAT antibody and quantified the number of motor neurons from the C7 spinal cord (Fig. 6a-f). I did not observe a significant difference in the number of motor neurons between 8-month-old *ChAT-Cre; Ankrd16$^{fl/-}$; Aars$^{sti/sti}$* and B6J mice (Fig. 6g).

To quantify the number of motor neurons in the lumbar region of the spinal cord, I switched to an indirect method of counting ventral root axons rather than counting motor neuron cell bodies since this method has been demonstrated to be a more reliable method for motor neuron quantification, i.e., if loss of motor neuron cell bodies is occurring, I should also see a decrease in the total number of axons exiting the ventral root (Burgess et al., 2010). I quantified the number of axons in the fifth lumbar vertebra (L5) ventral root which contains outgoing motor axons that exit the spinal cord to innervate muscles in the hindlimbs. The L5 ventral root for each genotype was collected by Alana Gibson. The L5 ventral root was then sent to The Jackson Laboratory for plastic embedding, sectioning, and staining. After I quantified the number of axons in the L5 ventral root of *ChAT-Cre; Ankrd16$^{fl/-}$; Aars$^{sti/sti}$*, *ChAT-Cre; Ankrd16$^{fl/-}$*, *Aars$^{sti/sti}$* and B6J mice, I did not see a significant difference in the total number of axons between any of the genotypes (Fig. 7a,b). Together, these results suggests that motor neuron death is not occurring in the cervical and lumbar regions of the spinal cord of *ChAT-Cre; Ankrd16$^{fl/-}$; Aars$^{sti/sti}$* mutants.

Ankrd16 loss in *Aars$^{sti/sti}$* motor neurons decreases the diameter of femoral axons.

To determine if the death of motor axons was occurring before the death of motor neurons in *ChAT-Cre; Ankrd16$^{fl/-}$; Aars$^{sti/sti}$* mice, the motor branch of the femoral nerve was collected by Alana Gibson. The femoral nerve was then sent to The Jackson Laboratory for plastic-embedding, sectioning, and staining. I then quantified the number of motor axons in the femoral nerve. The femoral nerve is derived from L2-L4 ventral roots and contains a motor branch that innervates the quadricep. By quantifying the femoral nerve, we can determine if peripheral neuropathy occurs even though motor neuron death was not detected. After

quantifying the total number of axons in the femoral nerve of *ChAT-Cre; Ankrd16$^{fl/-}$; Aars$^{sti/sti}$*, *Aars$^{sti/sti}$*, *ChAT-Cre; Ankrd16$^{fl/-}$*, and B6J mice, I did not see a significant difference in the total number of axons between any of the genotypes (Fig. 8a,b). These results demonstrate that peripheral neuropathy does not seem to occur in the femoral nerve of *ChAT-Cre; Ankrd16$^{fl/-}$; Aars$^{sti/sti}$* mutant mice.

Although no difference was observed in the total number of axons in the L5 ventral root and femoral nerve between *ChAT-Cre; Ankrd16$^{fl/-}$; Aars$^{sti/sti}$* and control mice, the diminished size of the axons in *ChAT-Cre; Ankrd16$^{fl/-}$; Aars$^{sti/sti}$* mutants (Fig. 7a, 8a) led me to measure the diameter of axons within the femoral nerve. Measuring axon diameters of the femoral nerve revealed a significant shift from larger axons to smaller axons in *ChAT-Cre; Ankrd16$^{fl/-}$; Aars$^{sti/sti}$* mutants, when compared to B6J mice (Fig. 9a). *ChAT-Cre; Ankrd16$^{fl/-}$; Aars$^{sti/sti}$* mice did not exhibit any axons greater than 9 µm and had a significantly lower number of axons between 7-9 µm, when compared to B6J mice (Fig. 9a). There is also a significant increase in the number of 3-5 µm axons in the nerve of *ChAT-Cre; Ankrd16$^{fl/-}$; Aars$^{sti/sti}$*, when compared to B6J mice, and a significant increase in axons ranging between 5-7 µm, when compared to B6J and *ChAT-Cre; Ankrd16$^{fl/-}$* mice (Fig. 9a). Although there is no significant difference between B6J and *Aars$^{sti/sti}$* mice, the number of larger axons of *Aars$^{sti/sti}$* mice appear to be trending downward similarly to *ChAT-Cre; Ankrd16$^{fl/-}$; Aars$^{sti/sti}$*, suggesting *Aars$^{sti/sti}$* may show an intermediate phenotype of decreased axonal size. These results suggest that conditional deletion of *Ankrd16* in motor neurons of *Aars$^{sti/sti}$* mice results in a decrease in diameter of the larger axons of *ChAT-Cre; Ankrd16$^{fl/-}$; Aars$^{sti/sti}$* femoral nerve.

In order for action potentials to travel properly along axons, myelination must be properly maintained. Given the fact that myelination problems are often linked with neurodegenerative

illnesses, we postulated that the shift towards smaller axons may be driven by alterations in myelination. To investigate any changes in myelination in the femoral nerve, I measured the g-ratio of these axons. The g-ratio is calculated by dividing the inner axon radius by the outer myelinated axon radius and can be used as an indicator of myelination changes. However, no changes were observed in the g-ratio of axons between genotypes (Fig. 9b). This data suggests that the shift from larger axons towards smaller axons in *ChAT-Cre; Ankrd16*$^{fl/-}$*; Aars*$^{sti/sti}$ mutants may be a result of other external factors outside of myelination that have yet to be discovered.

Discussion

Conditional deletion of *Ankrd16* may be useful for studying weight and muscle loss in neurological disorders.

Patients with neurodegenerative diseases frequently experience substantial weight loss as a result of muscular atrophy caused by inactivity and a physical inability to ingest enough calories. Unintentional weight reduction can also aggravate the symptoms of many neurological illnesses, leading to increased morbidity and mortality. We found that conditionally deleting *Ankrd16* in motor neurons of $Aars^{sti/sti}$ mice resulted in a substantial reduction in total body size and muscle weight in the triceps and gastrocnemius muscles, which was not attributable to a proportionate decline in body size. However, it is unclear if the decreased body weight and muscle weights in *ChAT-Cre;* $Ankrd16^{fl/-}$*;* $Aars^{sti/sti}$ mutant mice is the result of a loss of mass as the mice age, or if the body size and muscle weights are smaller at birth. Weights of mice and muscle weight-to-body weight ratios at earlier timepoints of each genotype would be needed to establish whether weight and muscle loss is happening. If weight and muscle loss is indeed occurring, conditional ablation of *Ankrd16* in motor neurons may be helpful for researching weight and muscle loss associated with various neurological disorders if further investigated.

The absence of NMJ denervation and motor neuron death in *ChAT-Cre;* $Ankrd16^{fl/-}$*;* $Aars^{sti/sti}$ mutant mice may suggest that decreased muscle mass in these mice may be caused by early aspects peripheral neuropathy induced by conditional deletion of *Ankrd16* in $Aars^{sti/sti}$ motor neurons. Although there were no significant changes in motor axon counts in the femoral nerve, it is possible that peripheral neuropathy is developing in regions other than the femoral

nerve. While NMJs were studied qualitatively, it may be worthwhile in future studies to quantify the number of NMJs present in mutant mice. We did not observe any obvious differences in NMJs of each genotype, but qualitative examination is not the best way to examine the possibility of fewer overall NMJs present caused by conditional deletion of *Ankrd16*.

Aars$^{sti/sti}$ motor neurons may be more resistant to loss of *Ankrd16* than other neurons.

Despite observing protein aggregation and subsequent cell death of Purkinje cells in *Aars*$^{sti/sti}$ mice owing to low levels of *Ankrd16*, and despite being able to generate cell type-specific protein aggregation and neurodegeneration caused by conditional *Ankrd16* deletion in *Aars*$^{sti/sti}$ forebrain neurons (Lee et al., 2006; Vo et al., 2018), we were unable to induce the death of motor neuronal cell bodies by conditional deletion of *Ankrd16* in the spinal cord of *Aars*$^{sti/sti}$ mice. The exact reason for cell death specificity in neuronal cell types has yet to be discovered but is critical for understanding and preventing neurodegenerative diseases. There are many different ways for neurons to die, including intrinsic and extrinsic apoptosis, ferroptosis, necroptosis, oncosis, parthanatos, autophagic cell death, and phagoptosis, and it may be possible that something that causes death in one cell type does not induce death in another cell type (Fricker et al., 2018). Motor neurons are some of the longest cells in the body, and they may contain a variety of methods to protect themselves against cell death caused by mistranslation and protein aggregation. It may be possible that motor neurons are more resistant to *Ankrd16* loss than other neuronal cell types and are resilient to conditionally deleting *Ankrd16* in the presence of the *sticky* mutation causing an editing-defective AlaRS. In future studies, it may be

worthwhile to investigate and test various mechanisms of cell death in motor neuron cell types in order to get a better understanding of cell type-specific death.

Axonal shrinkage may be causing the phenotypes observed in *ChAT-Cre; Ankrd16$^{fl/-}$; Aars$^{sti/sti}$* mutant mice.

Neuronal shrinkage has been seen in patients with degenerative neurological diseases such as Alzheimer's disease, Parkinson's disease, and Huntington's disease, among others (Huot et al., 2007; Mann et al., 1984). Some research suggests that shrinking neurons may result in impaired axonal transport, decreased axonal conduction velocities, and muscular denervation (Flood et al., 1999; Kiernan & Hudson, 1991). It has been shown that some ALS-causing mutations impair axonal transport (Alami et al., 2014). Regulation of axonal diameter is largely unknown, but has been suggested to be maintained by mechanisms involving the cytoskeleton (Costa et al., 2018). It is plausible that cytoskeletal dysfunction and/or axonal transport impairment may contribute to the smaller axon diameters observed in *ChAT-Cre; Ankrd16$^{fl/-}$; Aars$^{sti/sti}$* mutant mice, resulting in incorrect signaling at NMJs and muscle atrophy. Axonal transport impairment may explain why we see decreased muscle weights but do not observe loss of NMJs or peripheral neuropathy in *ChAT-Cre; Ankrd16$^{fl/-}$; Aars$^{sti/sti}$* mutant mice with shrinking neurons. In the future, it may be worthwhile to explore cytoskeletal dysfunctions, axonal transport, and impaired signaling at NMJs in *ChAT-Cre; Ankrd16$^{fl/-}$; Aars$^{sti/sti}$* mutant mice.

Earlier studies have shown that motor neurons of patients with ALS become smaller before they die (Kiernan & Hudson, 1993). Therefore, although we do not see motor neuron

death but we do find decreased axon diameters, it is conceivable that axons shrink first before motor neurons die in *ChAT-Cre; Ankrd16*$^{fl/-}$*; Aars*$^{sti/sti}$ mutant mice. Motor neuron death might be seen in *ChAT-Cre; Ankrd16*$^{fl/-}$*; Aars*$^{sti/sti}$ mutant mice if they were able to live longer. Although the precise cause of axonal shrinkage has yet to be discovered, it is possible that early detection of axonal shrinkage may be an early indication of neurological diseases.

Figures

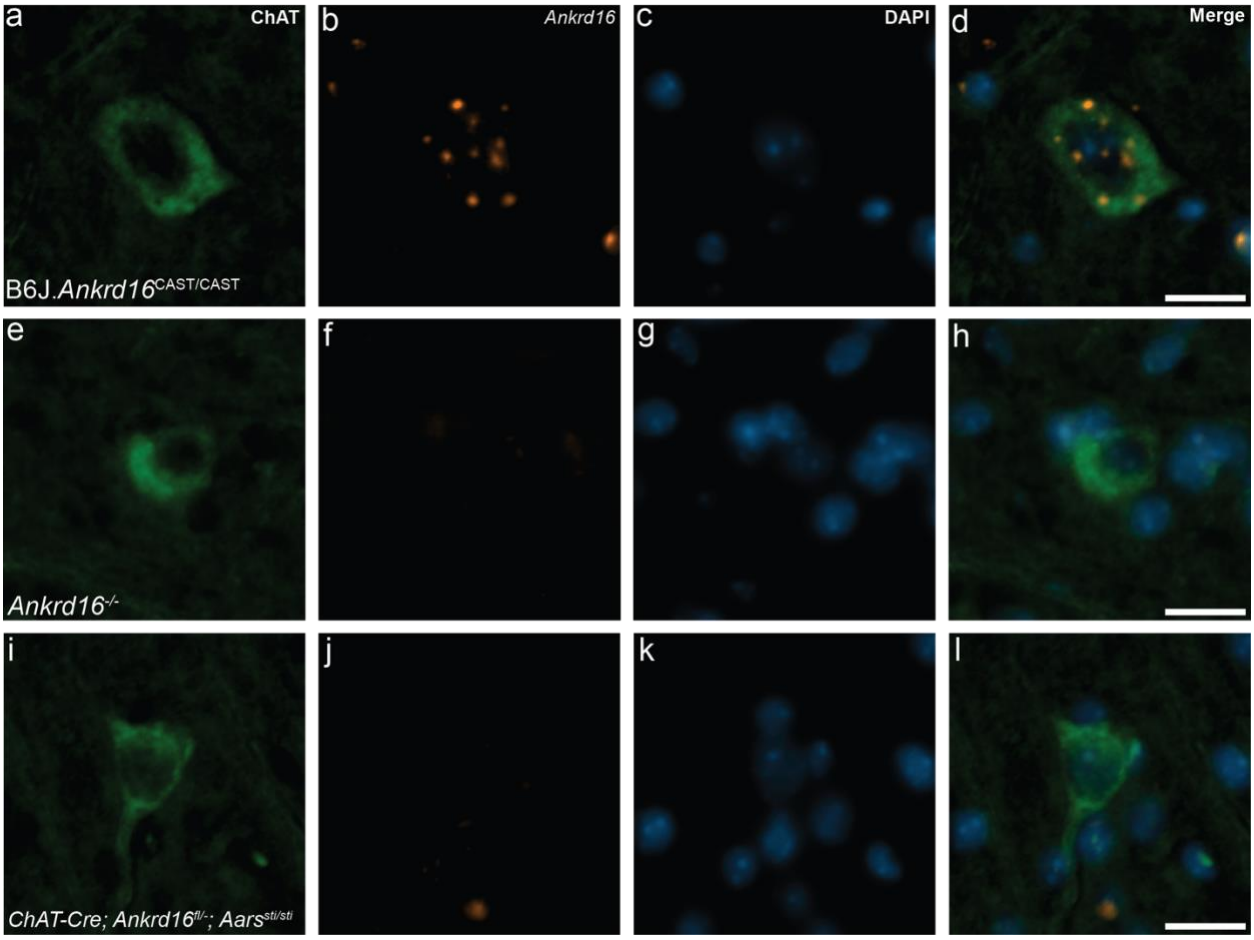

Figure 1: *Ankrd16* is conditionally deleted in *ChAT-Cre; Ankrd16$^{fl/-}$; Aars$^{sti/sti}$* mice.
a-l. BaseScope *in situ* hybridization of *Ankrd16* transcripts and immunofluorescence of ChAT-expressing motor neurons of B6J.*Ankrd16*$^{CAST/CAST}$ (n=1), *Ankrd16*$^{-/-}$ (n=1), and *ChAT-Cre; Ankrd16$^{fl/-}$; Aars$^{sti/sti}$* mice (n=1). (**a**, **e**, **i**) Immunofluorescence with antibodies to ChAT (green) labels motor neurons. (**b**, **f**, **j**) BaseScope probes label *Ankrd16* transcripts (orange) (**c**, **g**, **k**) DAPI labels the nuclei (blue) (**d**, **h**, **l**) BaseScope *in situ* hybridization, immunofluorescence of ChAT-positive motor neurons and DAPI merged into one image. Scale bars, 20 µm.

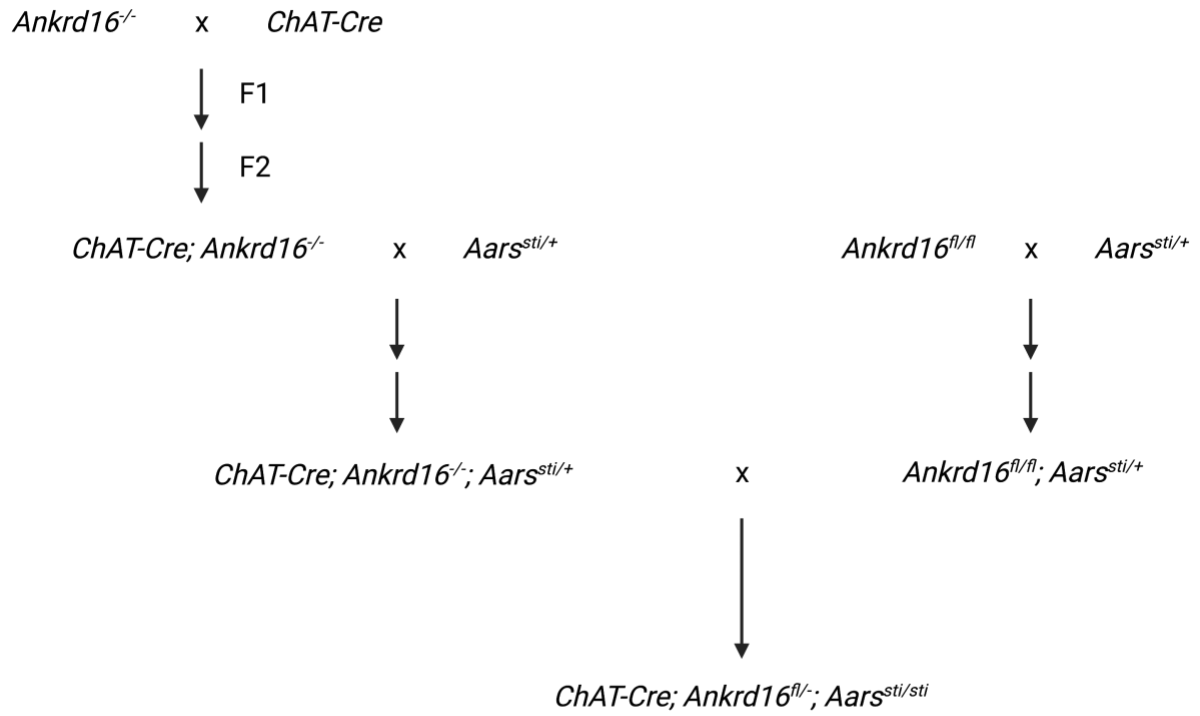

Figure 2: Generation of *ChAT-Cre; Ankrd16$^{fl/-}$; Aars$^{sti/sti}$* mice.
Ankrd16$^{-/-}$ and *ChAT*-Cre were used to generate *ChAT-Cre; Ankrd16$^{-/-}$*. *ChAT-Cre; Ankrd16$^{-/-}$* mice were crossed with *Aars$^{sti/+}$*, to generate *ChAT-Cre; Ankrd16$^{-/-}$; Aars$^{sti/+}$*. *Ankrd16$^{fl/fl}$* mice were then mated with *Aars$^{sti/+}$* to generate *Ankrd16$^{fl/fl}$; Aars$^{sti/+}$*. Lastly, *ChAT-Cre; Ankrd16$^{-/-}$; Aars$^{sti/+}$* mice were crossed with *Ankrd16$^{fl/fl}$; Aars$^{sti/+}$* to generate *ChAT-Cre; Ankrd16$^{fl/-}$; Aars$^{sti/sti}$*.

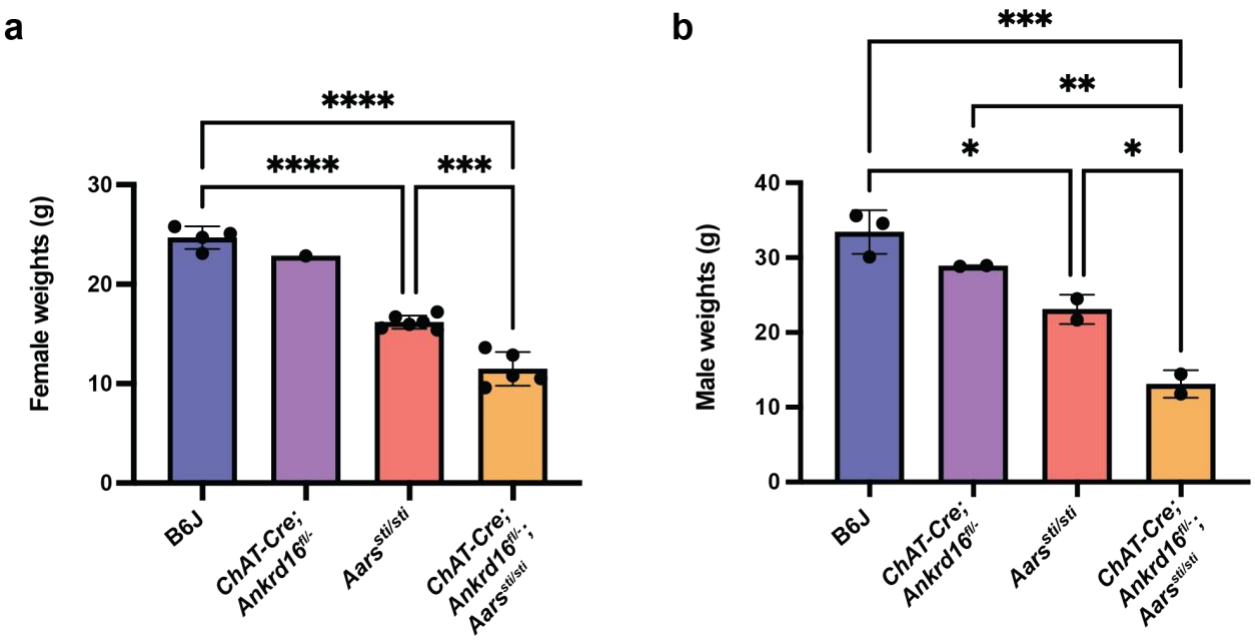

Figure 3: *ChAT-Cre; Ankrd16$^{fl/-}$; Aars$^{sti/sti}$* mice weigh less than controls.
a. Total body weights of 8-month-old female mice of the genotypes shown. **b.** Total body weights of 8-month-old male mice of each genotype. Bars and error bars are mean ± s.d., black circles represent weight from individual mice. One-way ANOVA (Tukey's test); p-value ≤ 0.05 (*), p-value ≤ 0.01 (**), p-value ≤ 0.001 (***), p-value ≤ 0.0001 (****).

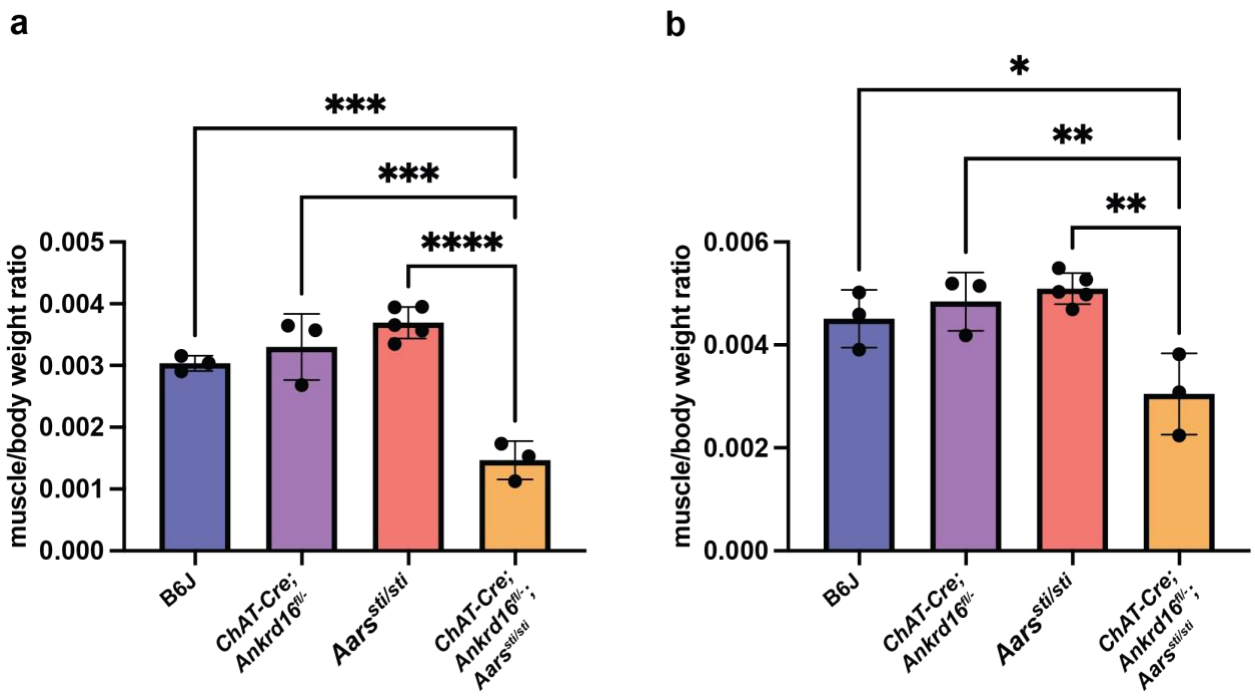

Figure 4: Muscles of *ChAT-Cre; Ankrd16$^{fl/-}$; Aars$^{sti/sti}$* mice are smaller than controls.
a. Ratio of triceps weight-to-body weight for each genotype at 8 months of age. Average of left and right triceps of each genotype were quantified. **b.** Ratio of gastrocnemius weight-to-body weight for each genotype at 8 months of age. Average of left and right gastrocnemius of each genotype were quantified. Bars and error bars are mean ± s.d., black circles represent average of left and right muscle-to-body weight ratio from individual mice. One-way ANOVA (Tukey's test), p-value ≤ 0.05 (*), p-value ≤ 0.01 (**), p-value ≤ 0.001 (***), p-value ≤ 0.0001 (****).

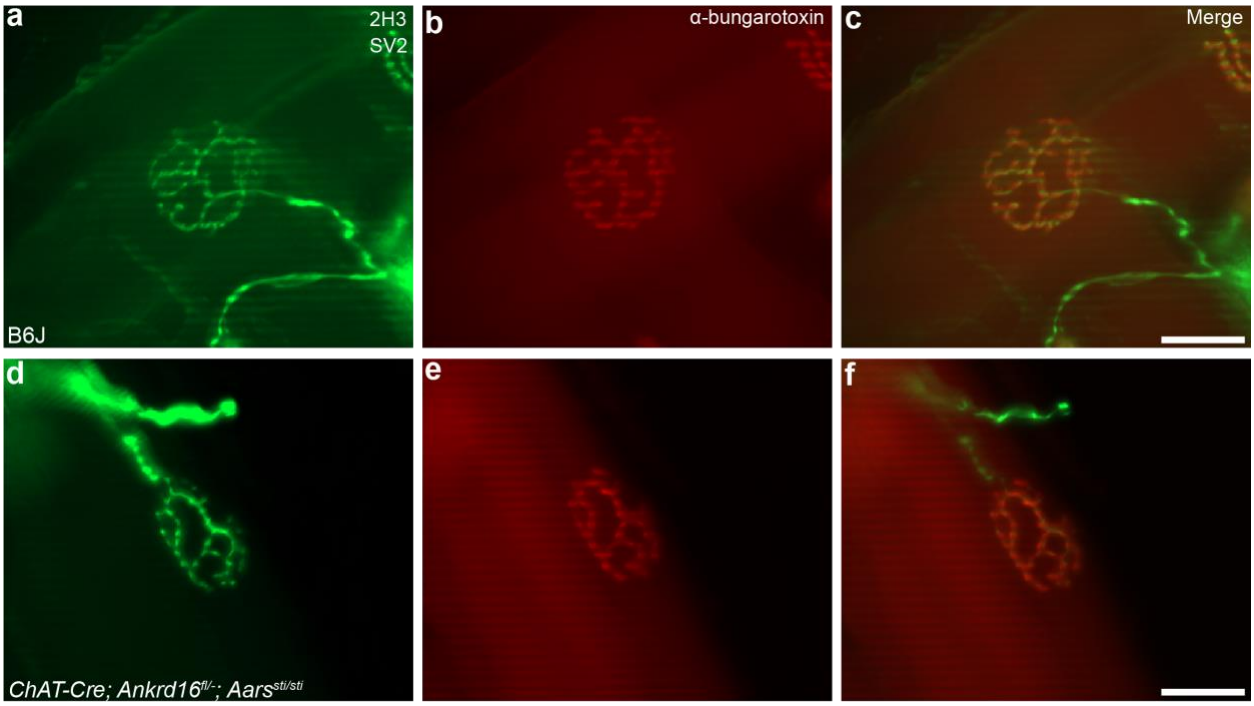

Figure 5: NMJ morphology appears normal in *ChAT-Cre; Ankrd16$^{fl/-}$; Aars$^{sti/sti}$* mice. **a-f.** Immunofluorescence of gastrocnemius NMJs of 8-month B6J and *ChAT-Cre; Ankrd16$^{fl/-}$; Aars$^{sti/sti}$* mice. (**a**, **d**) Immunofluorescence with antibodies to 2H3 and SV2 (green) labels the axons and presynaptic nerve terminals of the NMJs. (**b**, **e**) Immunofluorescence with α-bungarotoxin (red) labels the postsynaptic muscle end plate of the NMJs. (**c**, **f**) Immunofluorescence of presynaptic nerve terminal and postsynaptic muscle end plate merged into one image. Scale bars, 10 μm.

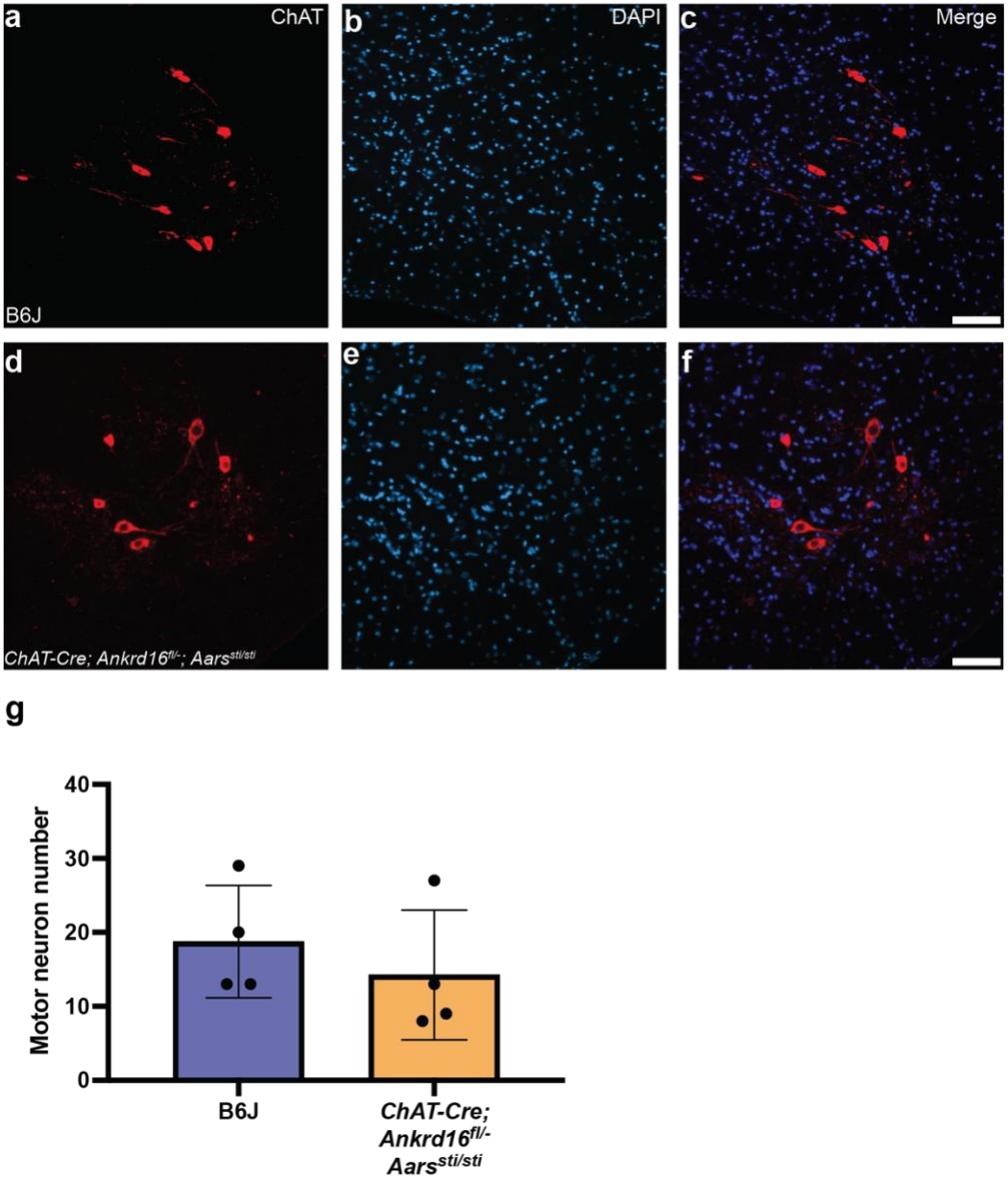

Figure 6: No apparent loss of lower motor neurons in *ChAT-Cre; Ankrd16$^{fl/-}$; Aars$^{sti/sti}$* mice. **a-f.** Immunofluorescence of ChAT-expressing motor neurons of 8-month B6J and *ChAT-Cre; Ankrd16$^{fl/-}$; Aars$^{sti/sti}$* mice. (**a**, **d**) Immunofluorescence with antibodies to ChAT (red) labels motor neurons. (**b**, **e**) DAPI labels the nuclei (blue). (**c**, **f**) Immunofluorescence of ChAT-positive motor neurons and DAPI merged into one image. Scale bars, 100 µm. **g.** Quantification of motor neurons of the C7 region of the spinal cord in 8-month-old B6J (n=4) and *ChAT-Cre; Ankrd16$^{fl/-}$; Aars$^{sti/sti}$* mice (n=4). Bars and error bars are mean ± s.d., each black circle represents the average number of motor neurons counted from three C7 sections of an individual mouse. Welch's t test.

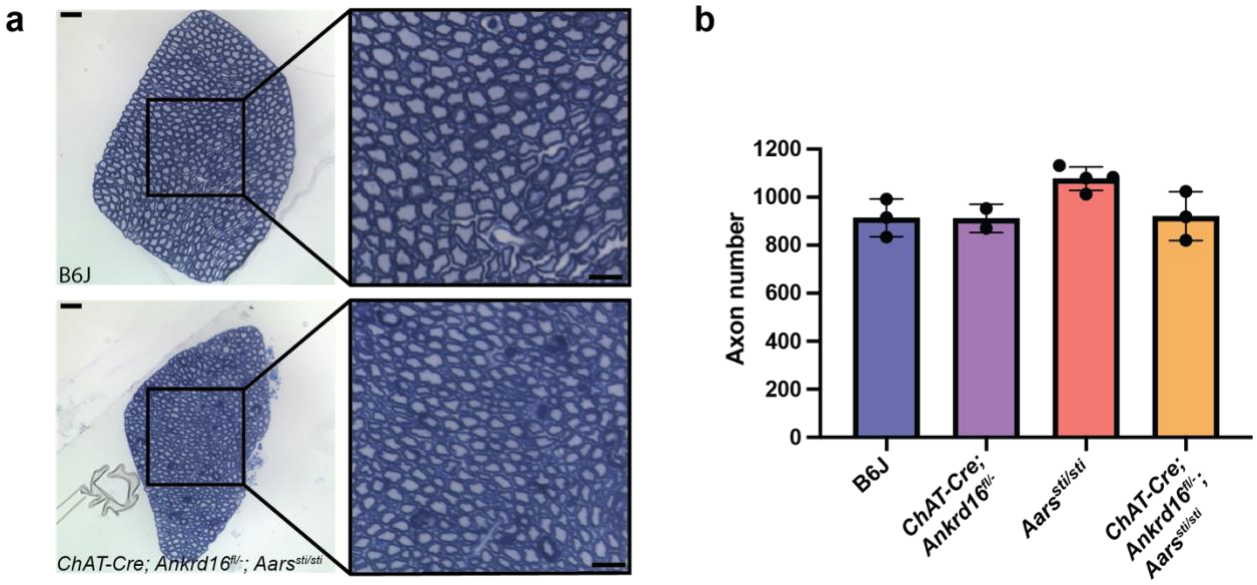

Figure 7: No loss of motor neurons in *ChAT-Cre; Ankrd16$^{fl/-}$; Aars$^{sti/sti}$* mice detected by L5 ventral root analysis.

a. Cross-section of L5 ventral root stained with Toluidine Blue of 8-month B6J and *ChAT-Cre; Ankrd16$^{fl/-}$; Aars$^{sti/sti}$* mice. Lower magnification and higher magnification of boxed area. **b.** Total axon count of the L5 ventral root of each genotype at 8 months of age. Bars and error bars are mean ± s.d., each black circle represents the total axon number in one L5 ventral root from an individual mouse. One-way ANOVA (Tukey's test). Scale bars, lower magnification 20 µm, higher magnification 10 µm.

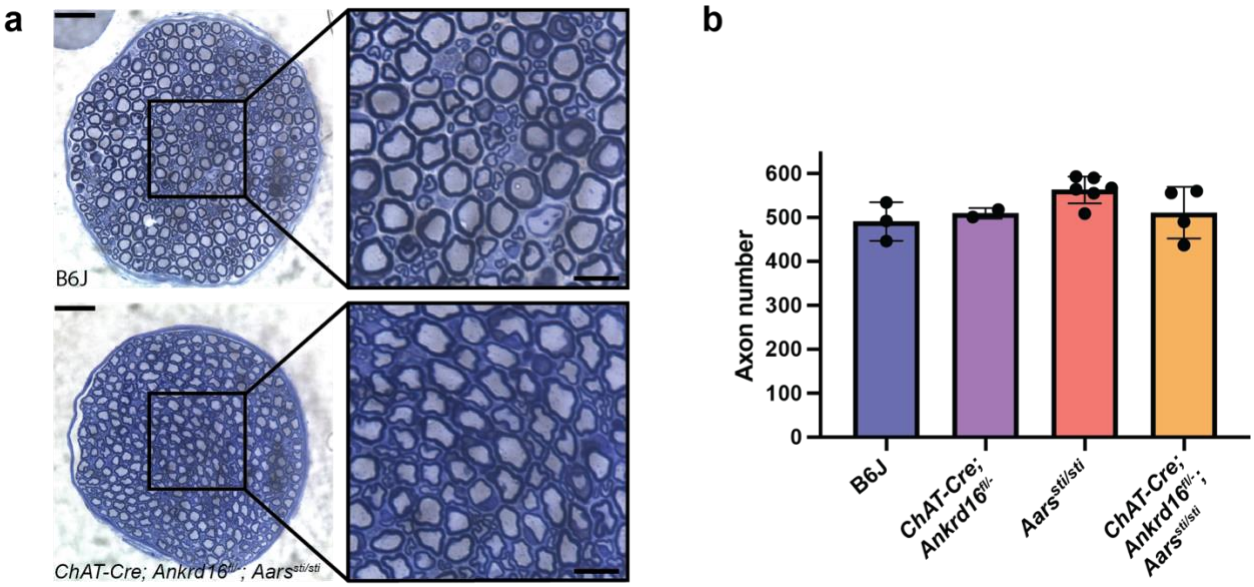

Figure 8: No loss of axons detected in the femoral nerve of *ChAT-Cre; Ankrd16$^{fl/-}$; Aars$^{sti/sti}$* mice.

a. Cross-section of femoral nerve stained with Toluidine Blue of 8-month-old wild-type B6J and *ChAT-Cre; Ankrd16$^{fl/-}$; Aars$^{sti/sti}$* mice. Lower magnification and higher magnification of boxed area. **b.** The number of axons in the femoral nerve of each genotype at 8 months of age. Bars and error bars are mean ± s.d., each black circle represents the total axon number in one femoral nerve from an individual mouse. One-way ANOVA (Tukey's test). Scale bars, lower magnification 20 µm, higher magnification 10 µm.

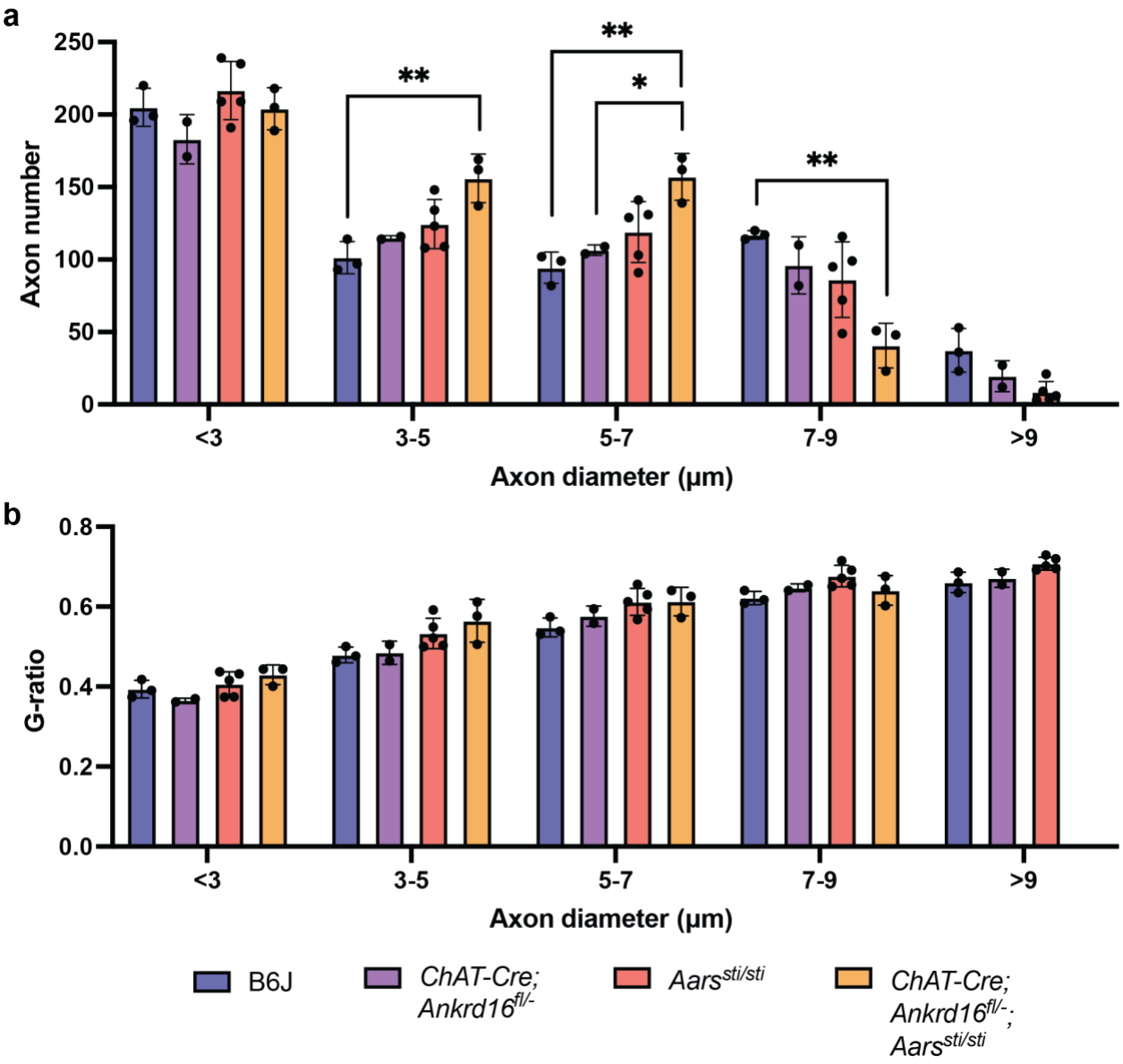

Figure 9: Decrease in diameter of larger femoral axons of *ChAT-Cre; Ankrd16$^{fl/-}$; Aars$^{sti/sti}$* mice.

a. Quantification of the number of axons of the femoral nerve of each genotype at 8 months of age grouped by axon diameter (µm). Bars and error bars are mean ± s.d., each black circle represents the total axon number per diameter bin from one femoral nerve of an individual mouse. One-way ANOVA (Tukey's test), p-value ≤ 0.05 (*), p-value ≤ 0.01 (**). **b.** G-ratio of axons of the femoral nerve of each genotype at 8 months of age grouped by axon diameter (µm). Bars and error bars are mean ± s.d., each black circle represents the average g-ratio for all axons within one femoral nerve of an individual mouse. One-way ANOVA (Tukey's test).

References

Alami, N. H., Smith, R. B., Carrasco, M. A., Williams, L. A., Winborn, C. S., Han, S. S. W., Kiskinis, E., Winborn, B., Freibaum, B. D., Kanagaraj, A., Clare, A. J., Badders, N. M., Bilican, B., Chaum, E., Chandran, S., Shaw, C. E., Eggan, K. C., Maniatis, T., & Taylor, J. P. (2014). Axonal Transport of TDP-43 mRNA Granules Is Impaired by ALS-Causing Mutations. *Neuron*, *81*(3), 536–543. https://doi.org/10.1016/j.neuron.2013.12.018

Benkler, C., O'Neil, A. L., Slepian, S., Qian, F., Weinreb, P. H., & Rubin, L. L. (2018). Aggregated SOD1 causes selective death of cultured human motor neurons. *Scientific Reports*, *8*(1), 1–14. https://doi.org/10.1038/s41598-018-34759-z

Burgess, R. W., Cox, G. A., & Seburn, K. L. (2010). Neuromuscular Disease Models and Analysis. In *Methods in Molecular Biology* (Vol. 602). https://doi.org/10.1007/978-1-60761-058-8_20

Costa, A. R., Pinto-Costa, R., Sousa, S. C., & Sousa, M. M. (2018). The Regulation of Axon Diameter: From Axonal Circumferential Contractility to Activity-Dependent Axon Swelling. *Frontiers in Molecular Neuroscience*, *11*(September), 1–7. https://doi.org/10.3389/fnmol.2018.00319

Davis, M., & Stroud, C. (2013). *Neurodegeneration: Exploring Commonalities Across Diseases: Workshop Summary* (1st edition). National Academies Press. https://doi.org/10.17226/18341

Dulic, M., Cvetesic, N., Perona, J. J., & Gruic-Sovulj, I. (2010). Partitioning of tRNA-dependent editing between pre- and post-transfer pathways in class I aminoacyl-tRNA synthetases. *Journal of Biological Chemistry*, *285*(31), 23799–23809. https://doi.org/10.1074/jbc.M110.133553

Flood, D. G., Reaume, A. G., Gruner, J. A., Hoffman, E. K., Hirsch, J. D., Lin, Y. G., Dorfman, K. S., & Scott, R. W. (1999). Hindlimb motor neurons require Cu/Zn superoxide dismutase for maintenance of neuromuscular junctions. *American Journal of Pathology*, *155*(2), 663–672. https://doi.org/10.1016/S0002-9440(10)65162-0

Frade, J. M., & Ovejero-Benito, M. C. (2015). Neuronal cell cycle: The neuron itself and its circumstances. *Cell Cycle*, *14*(5), 712–720. https://doi.org/10.1080/15384101.2015.1004937

Fricker, M., Tolkovsky, A. M., Borutaite, V., Coleman, M., & Brown, G. C. (2018). Neuronal cell death. *Physiological Reviews*, *98*(2), 813–880. https://doi.org/10.1152/physrev.00011.2017

Giegé, R., Sissler, M., & Florentz, C. (1998). Universal rules and idiosyncratic features in tRNA identity. *Nucleic Acids Research*, *26*(22), 5017–5035. https://doi.org/10.1093/nar/26.22.5017

Guo, M., Chong, Y. E., Shapiro, R., Beebe, K., Yang, X. L., & Schimmel, P. (2009). Paradox of mistranslation of serine for alanine caused by AlaRS recognition dilemma. *Nature*, *462*(7274), 808–812. https://doi.org/10.1038/nature08612

Hopfield, J. J. (1974). Kinetic Proofreading: A New Mechanism for Reducing Errors in Biosynthetic Processes Requiring High Specificity. *Proceedings of the National Academy of Sciences of the United States of America*, *71*(10), 4135–4139.

Huot, P., Lévesque, M., & Parent, A. (2007). The fate of striatal dopaminergic neurons in Parkinson's disease and Huntington's chorea. *Brain*, *130*(1), 222–232. https://doi.org/10.1093/brain/awl332

Jakubowski, H., & Goldman, E. (1992). Editing of errors in selection of amino acids for protein synthesis. *Microbiological Reviews*, *56*(3), 412–429. https://doi.org/10.1128/mmbr.56.3.412-429.1992

Kiernan, J. A., & Hudson, A. J. (1991). Changes in sizes of cortical and lower motor neurons in amyotrophic lateral sclerosis. *Brain*, *114*(2), 843–853. https://doi.org/10.1093/brain/114.2.843

Kiernan, J. A., & Hudson, A. J. (1993). Changes in shapes of surviving motor neurons in amyotrophic lateral sclerosis. *Brain*, *116*(1), 203–215. https://doi.org/10.1093/brain/116.1.203

Lee, J. W., Beebe, K., Nangle, L. A., Jang, J., Longo-Guess, C. M., Cook, S. A., Davisson, M. T., Sundberg, J. P., Schimmel, P., & Ackerman, S. L. (2006). Editing-defective tRNA synthetase causes protein misfolding and neurodegeneration. *Nature*, *443*(7107), 50–55. https://doi.org/10.1038/nature05096

Mann, D. M. A., Yates, P. O., & Marcyniuk, B. (1984). Relationship between pigment accumulation and age in Alzheimer's disease and Down syndrome. *Acta Neuropathologica*, *63*(1), 72–77. https://doi.org/10.1007/BF00688473

Martinis, S. A., & Boniecki, M. T. (2008). The balance between pre- and post-transfer editing in tRNA synthetases. *FEBS Lett.*, *23*(1), 1–7. https://doi.org/10.1016/j.febslet.2009.11.071.The

Moras, D. (2010). Proofreading in translation: Dynamics of the double-sieve model. *Proceedings of the National Academy of Sciences of the United States of America*, *107*(51), 21949–21950. https://doi.org/10.1073/pnas.1016083107

Newberry, K. J., Hou, Y., & Perona, J. J. (2002). Structural origins of amino acid selection without editing by cysteinyl-tRNA synthetase. *The EMBO Journal*, *21*(11), 2778–2787.

Pang, Y. L. J., Poruri, K., & A. Martinis, S. (2014). tRNA sytherase: tRNA Aminoacylation and beyond. *Wiley Interdisciplinary Reviews. RNA*, *5*(4), 461–480. https://doi.org/10.1002/wrna.1224.tRNA

Schramm, F. D., Schroeder, K., Alvelid, J., Testa, I., & Jonas, K. (2019). Growth-driven displacement of protein aggregates along the cell length ensures partitioning to both daughter cells in Caulobacter crescentus. *Molecular Microbiology*, *111*(6), 1430–1448. https://doi.org/10.1111/mmi.14228

Sokabe, M., Ose, T., Nakamura, A., Tokunaga, K., Nureki, O., Yao, M., & Tanaka, I. (2009). The structure of alanyl-tRNA synthetase with editing domain. *Proceedings of the National Academy of Sciences of the United States of America*, *106*(27), 11028–11033. https://doi.org/10.1073/pnas.0904645106

Vo, M. N., Terrey, M., Lee, J. W., Roy, B., Moresco, J. J., Sun, L., Fu, H., Liu, Q., Weber, T. G., Yates, J. R., Fredrick, K., Schimmel, P., & Ackerman, S. L. (2018). ANKRD16 prevents neuron loss caused by an editing-defective tRNA synthetase. *Nature*, *557*(7706), 510–515. https://doi.org/10.1038/s41586-018-0137-8

Wang, F., Flanagan, J., Su, N., Wang, L. C., Bui, S., Nielson, A., Wu, X., Vo, H. T., Ma, X. J., & Luo, Y. (2012). RNAscope: A novel in situ RNA analysis platform for formalin-fixed, paraffin-embedded tissues. *Journal of Molecular Diagnostics*, *14*(1), 22–29. https://doi.org/10.1016/j.jmoldx.2011.08.002